Soft Matter

Accepted Manuscript

This is an *Accepted Manuscript*, which has been through the Royal Society of Chemistry peer review process and has been accepted for publication.

Accepted Manuscripts are published online shortly after acceptance, before technical editing, formatting and proof reading. Using this free service, authors can make their results available to the community, in citable form, before we publish the edited article. We will replace this *Accepted Manuscript* with the edited and formatted *Advance Article* as soon as it is available.

You can find more information about *Accepted Manuscripts* in the Information for Authors.

Please note that technical editing may introduce minor changes to the text and/or graphics, which may alter content. The journal's standard Terms & Conditions and the Ethical guidelines still apply. In no event shall the Royal Society of Chemistry be held responsible for any errors or omissions in this *Accepted Manuscript* or any consequences arising from the use of any information it contains.

ROYAL SOCIETY OF CHEMISTRY

www.rsc.org/softmatter

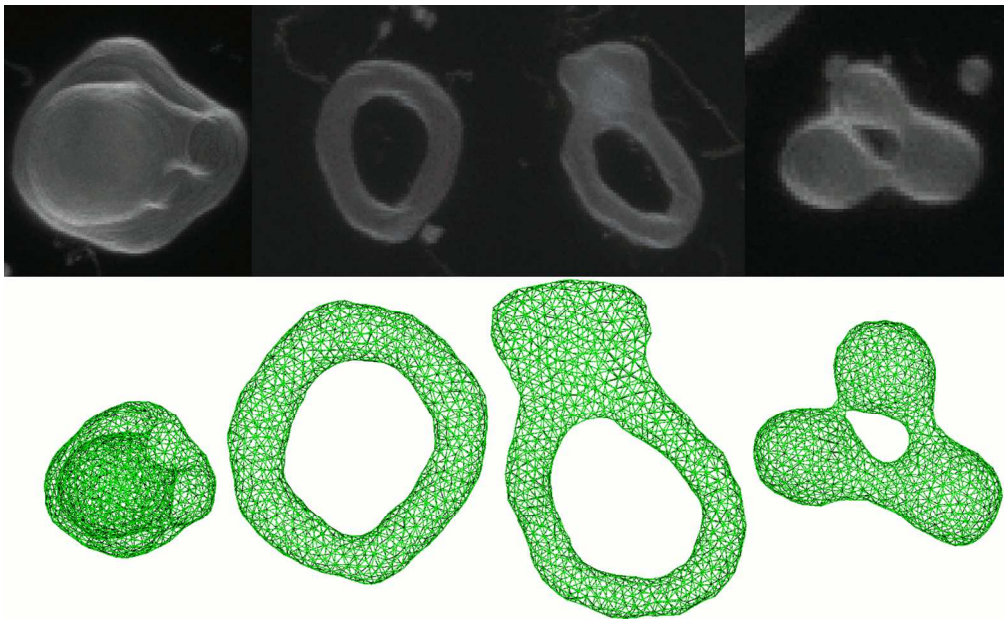

Morphologies of genus-1 toroidal vesicles
496x304mm (72 x 72 DPI)

Soft Matter Accepted Manuscript

ARTICLE TYPE
www. rsc.org/xxxxxx | XXXXXXXX

Shape transformations of toroidal vesicles†

Hiroshi Noguchi [a,*], **Ai Sakashita**[a,b], **and Masayuki Imai**[c]

Received 25th August 2014, Accepted 16th October 2014
First published on the web Xth XXXXXXXXXX 2014
DOI: 10.1039/b000000x

Morphologies of genus-1 and 2 toroidal vesicles are studied numerically by dynamically triangulated membrane models and experimentally by confocal laser microscopy. Our simulation results reproduce shape transformations observed in our experiments well. At large reduced volumes of the genus-1 vesicles, obtained vesicle shapes agree with the previous theoretical prediction, in which axisymmetric shapes are assumed: double-necked stomatocyte, discoidal toroid, and circular toroid. However, for small reduced volumes, it is revealed that a non-axisymmetric discoidal toroid and handled discocyte exist in thermal equilibrium in the parameter range, in which the previous theory predicts axisymmetric discoidal shapes. Polygonal toroidal vesicles and subsequent budding transitions are also found. The entropy caused by shape fluctuations slightly modifies the stability of the vesicle shapes.

1 Introduction

Vesicles are closed bilayer membranes that show a wide variety of morphologies depending on the lipid architecture as well as their environment. Since fluid lipid membranes are the main component of biomembranes, lipid vesicles are considered as a simple model system of cells. In particular, vesicle shapes with genus $g = 0$ have been intensively investigated and are well understood[1–9]. For example, the shape of red blood cells, discocyte, can be formed by a lipid membrane without proteins. In contrast to the genus-0 vesicles, vesicles with nonzero genus have been much less explored. In this paper, we focus on vesicles with $g = 1$ and $g = 2$.

In living cells, organelles exist in various shapes. In some organelles, lipidic necks or pores connect biomembranes such that they have nonzero genus. For example, the nuclear membrane and endoplasmic reticulum are connected and together form complicated shapes. The nucleus is wrapped by two bilayer membranes connected by many lipidic pores. Thus, its shape is considered as a stomatocyte of a high-genus vesicle connected with a tubular network. It is important to understand how their topologies affect their morphologies.

Vesicle shapes are determined by the curvature energy and the area difference ΔA of two monolayers of bilayer membranes with a constraint on the reduced volume V^* [1–4], which is the volume relative to a spherical vesicle of the same surface area. It is defined as $V^* = V/(4\pi/3){R_\mathrm{A}}^3$ with $R_\mathrm{A} = \sqrt{A/4\pi}$, where V and A are the vesicle volume and surface area, respectively. Since transverse diffusion (flip–flop) of phospholipids between two monolayers is very slow, the number difference ΔN_lip of lipids between two monolayers can be conserved on a typical experimental time scale. In the bilayer coupling (BC) model, the area difference ΔA is fixed as the preferred value $\Delta A_0 = \Delta N_\mathrm{lip} a_\mathrm{lip}$, where a_lip is the area per lipid in tensionless membranes. In the area-difference-elasticity (ADE) model, a harmonic potential for the difference $\Delta A - \Delta A_0$ is added as a penalty for the deviation of the area difference. For genus-0 vesicles, various observed morphologies can be reproduced well by both BC and ADE models[1–4]: stomatocyte, discocyte, prolate, pear, pearl-necklace, and branched starfish-like shapes. However, shape-transformation dynamics is better explained by the ADE model[8].

The vesicle shapes with $g = 1$ and $g = 2$ were studied in the 1990s[10–18]. For $g = 1$, the phase diagrams of axisymmetric shapes were constructed for the BC, ADE, and spontaneous-curvature models by Jülicher et al.[13]. They assumed axisymmetry of the vesicle shape and the region of non-axisymmetric shapes is only estimated by a stability analysis of the axisymmetric shapes. However, the stability is only examined with respect to special conformal transformations and non-axisymmetric shapes were not directly explored. Thus, the full phase diagram of genus-1 vesicles has not been completed. For $g = 2$, conformational degeneracy was found in the ground state at $V^* \gtrsim 0.7$, where the vesicles can transform their shapes without changing their curvature energy with fixed V^* and ΔA [14,15,17]. In this paper, we revisit the phase diagram of $g = 1$ using three-dimensional simulations and find non-axisymmetric thermal-equilibrium shapes in the region

[a] *Institute for Solid State Physics, University of Tokyo, Kashiwa, Chiba 277-8581, Japan; E-mail: noguchi@issp.u-tokyo.ac.jp*
[b] *Department of Physics, Ochanomizu University, 2-1-1 Otsuka, Bunkyo, Tokyo 112-8610, Japan*
[c] *Department of Physics, Faculty of Science, Tohoku University, 6-3 Aramaki, Aoba-ku, Sendai, Miyagi 980-8578, Japan*
† Electronic Supplementary Information (ESI) available: See DOI: 10.1039/b000000x/

Soft Matter Accepted Manuscript

where axisymmetric shapes were assumed in Ref.[13]. In all of the previous theoretical studies on non-zero genus vesicle, the thermal fluctuations are neglected. However, experimentally, neck diffusion of toroidal vesicles and bending and length fluctuations of lipid tubes were reported[16,19,20]. We also investigate the effects of thermal fluctuations and compare our simulation results with shape transformations observed in our experiments for $g = 1$ and 2.

The simulation and experimental methods are provided in Sec. 2. In Sec. 3.1, vesicle shapes at $g = 1$ are described. First, the stable states for the curvature energy without the bilayer-coupling constraint or ADE energy is explained as a starting point. Subsequently the free-energy profiles are calculated for three values of the reduced volume. This calculation clarifies discrete shape transitions from non-axisymmetric discoidal shapes to circular toroids in the ADE model. The simulation results are compared with experimental images. The budding transitions are also discussed. In Sec. 3.2 the results for $g = 2$ are described. The summary and conclusions are given in Sec. 4.

2 Materials and Methods

2.1 Dynamically Triangulated Membrane Model

We employ a dynamically triangulated surface model to describe a fluid membrane[7,21,22]. The vesicle consists of $N_{\rm mb}$ vertices connected by bonds (tethers) to form a triangular network. The vertices have a hard-core excluded volume of diameter σ_0. The maximum length of the bond is σ_1. In order to keep the volume V and surface area A constant, harmonic potentials $U_{\rm V} = (1/2)k_{\rm V}(V - V_0)^2$ and $U_{\rm A} = (1/2)k_{\rm A}(A - A_0)^2$ are employed. A Metropolis Monte Carlo (MC) method is used to move vertices.

The curvature energy of a single-component fluid vesicle is given by[23,24]

$$U_{\rm cv} = \int \frac{\kappa}{2}(C_1 + C_2)^2 dA, \tag{1}$$

where C_1 and C_2 are the principal curvatures at each point in the membrane. The coefficient κ is the bending rigidity. The spontaneous curvature vanishes when lipids are symmetrically distributed in both monolayers of the bilayer. The integral over the Gaussian curvature C_1C_2 is omitted because it is invariant for a fixed topology.

In the ADE model, the ADE energy $U_{\rm ADE}$ is added[1–5]:

$$U_{\rm ADE} = \frac{\pi k_{\rm ade}}{2Ah^2}(\Delta A - \Delta A_0)^2. \tag{2}$$

The areas of the outer and inner monolayers of a bilayer vesicle differ by $\Delta A = h\int(C_1 + C_2)dA$, where h is the distance between the two monolayers. The BC model can be considered as the ADE model with $k_{\rm ade} = \infty$. The area differences are normalized by a spherical vesicle as $\Delta a = \Delta A/8\pi hR_{\rm A}$ and $\Delta a_0 = \Delta A_0/8\pi hR_{\rm A}$ to display our results. For the spherical vesicle with $\Delta a_0 = 0$, $\Delta a = 1$ and $U_{\rm ADE} = 8\pi^2 k_{\rm ade}$.

The mean curvature at the i-th vertex is discretized as[22,25,26]

$$(C_1 + C_2)\mathbf{n}_i = \frac{1}{\lambda_i}\sum_{j(i)}\frac{\lambda_{i,j}\mathbf{r}_{i,j}}{r_{i,j}}, \tag{3}$$

where the sum over $j(i)$ is for the neighbors of the i-th vertex, which are connected by bonds. The bond vector between the vertices i and j is $\mathbf{r}_{i,j}$, and $r_{i,j} = |\mathbf{r}_{i,j}|$. The length of a bond in the dual lattice is $\lambda_{i,j} = r_{i,j}[\cot(\theta_1) + \cot(\theta_2)]/2$. The angles θ_1 and θ_2 are opposite to bond ij in the two triangles sharing this bond, and $\lambda_i = 0.25\sum_{j(i)}\lambda_{i,j}r_{i,j}$ is the area of the dual cell. The normal vector $\mathbf{n}_i$ points from inside of the vesicle to outside.

The bonds are reconstructed by flipping them to the diagonal of two adjacent triangles using the Metropolis MC procedure. Triangle formation of the bonds outside of the membrane surface is rejected such that the minimum pore in vesicles consists of four bonds [see the middle snapshot in Fig. 1(a)]. In the present simulations, we use $N_{\rm mb} = 1000$, $\sigma_1/\sigma_0 = 1.67$, $k_{\rm V} = 4$, $k_{\rm A} = 8$, and $\kappa = 20k_{\rm B}T$, where $k_{\rm B}T$ is the thermal energy. The deviations of reduced volume V^* from the specified values are less than 0.01. We primarily use $k^*_{\rm ade} = k_{\rm ade}/\kappa = 1$, which is a typical value for phospholipids[3,8]. In the previous study[13], the phase diagram of genus-1 vesicles was constructed using this value.

The canonical MC simulations of the ADE model are performed with various parameter sets for the potential $U = U_{\rm cv} + U_{\rm V} + U_{\rm A} + U_{\rm ADE}$. To obtain the thermal equilibrium states, one of the generalized ensemble MC methods[26–28] is employed for genus-1 vesicles. Instead of the ADE potential $U_{\rm ADE}$, a weight potential $U_{\rm w}(\Delta A)$ is employed for a flat probability distribution over ΔA. Since the weight potential $U_{\rm w}(\Delta A)$ is not known a priori, it has to be estimated using an iterative procedure. After long simulations, the canonical ensemble of the ADE model is obtained by a re-weighting procedure[29]. In the case of the BC model, the canonical ensemble for the potential $U_0 = U_{\rm cv} + U_{\rm V} + U_{\rm A}$ is calculated for a small bin of Δa with a bin width of 0.0025. We perform annealing simulation to $T = 0$ and the canonical MC simulations with $N_{\rm mb} = 4000$ at several parameter sets to confirm the energy-minimum shapes and the finite size effects of the triangulation, respectively.

2.2 Experimental Method

We prepared single-component vesicles from DOPC (1,2-dioleoyl-sn-glycero-3-phosphocholine, Avanti Polar Lipids)

Soft Matter Accepted Manuscript

This journal is © The Royal Society of Chemistry [year]

using the gentle hydration method with deionized water[8]. TR-DHPE (Texas Red, 1,2-dihexadecanoyl-sn-glycero-3-phosphoethanolamine, Molecular Probes) was used as the dye (1% mole ratio). We kept vesicle suspensions at room temperature (24-25°C) and observed them using a fast confocal laser microscope (Carl Zeiss, LSM 5Live). At this stage, most vesicles spontaneously formed either a spherical or tubular shape. We observed vesicles with genus $g = 1$ or 2 by analyzing numerous microscopy images.

We observed shape transformations of the vesicles of $g = 1$ and 2. The intrinsic area difference Δa_0 is varied without changing the osmotic pressure. In Ref.[8], we calculated V, A, and Δa using the 3D images of genus-0 liposomes and found that during shape transformations, Δa is changed, whereas V and A are constant. We concluded that small lipid reservoirs such as small lipid aggregates and bicelles are likely present on the membrane, and the laser illumination of the microscope induces fusion into either monolayer of the lipid bilayer, which leads to changes in Δa_0. We applied this method to toroidal vesicles here. It is difficult to measure 3D shapes of the observed toroidal vesicles owing to smallness of the liposomes or low contrast of the images. It is not distinguishable only from the experiments whether observed shapes are in thermal equilibrium or in metastable state. We compare the experimental vesicle images and simulation snapshots and determine that they are in equilibrium or not.

3 Results and Discussions

3.1 Genus-1 Toroidal Vesicles

3.1.1 Curvature Energy Model. First, we compare the (meta-) stable shapes of genus-1 vesicles and genus-0 vesicles without the ADE energy or the BC constraint (see Fig. 1). The vesicles are simulated for the potential U_0. We call this model the curvature energy model. For the genus-0 vesicles, three axisymmetric shapes–stomatocyte, discocyte, and prolate– are formed. It is known that stomatocyte, discocyte, and prolate are the global-energy-minimum states for $0 < V^* < 0.59$, $0.59 < V^* < 0.65$, and $0.65 < V^* < 1$, respectively[3]. The shape transformations between these shapes are discrete transitions such that these shapes exist as metastable states in wider ranges of V^*. The free-energy-minimum states including metastable shapes are indicated by the blue lines in Fig. 1(b).

The genus-1 vesicles also have three energy-minimum shapes. For stomatocyte and discocyte, an additional small neck or pore appears. Instead of the prolate, a circular toroid is formed. Here, we abbreviate the shapes as 'sto,' 'disk,' and 'ring' for stomatocyte, discocyte, and circular toroid, respectively. The discocyte exists in a narrower range of V^* for $g = 1$ than for $g = 0$ [see Fig. 1(b)]. The previous theoretical study[11]

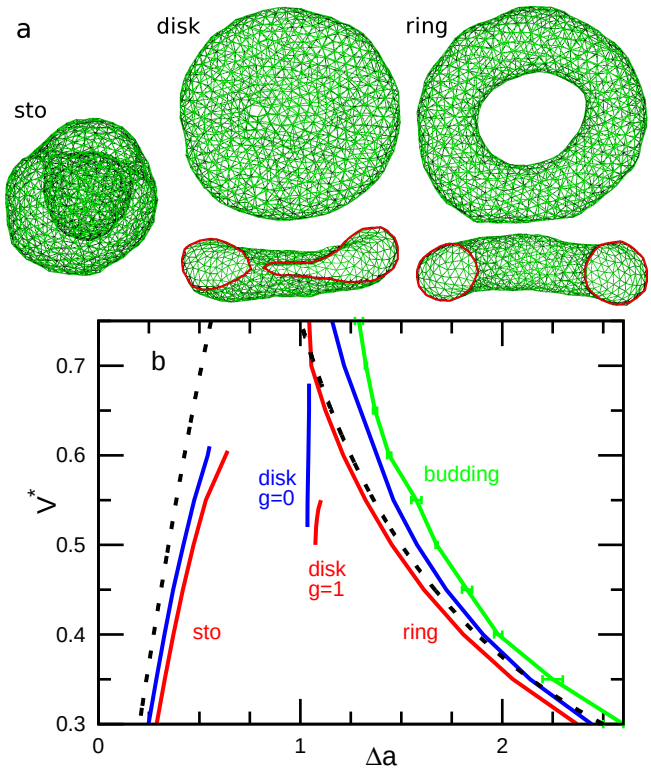

Fig. 1 Stable and meta-stable shapes of vesicles in the curvature energy model. (a) Snapshots of vesicles of genus $g = 1$ at $V^* = 0.5$. The labels 'sto,' 'disk,' and 'ring' represent stomatocyte, discocyte, and circular toroids, respectively. The side views of half-cut snapshots are also shown for disk and ring shapes. (b) Area difference Δa of (meta-) stable shapes at (red) $g = 1$ and (blue) $g = 0$. The green solid line represents Δa at the budding transition. The dashed black lines are the results obtained using simple geometrical models for stomatocye and ring shapes.

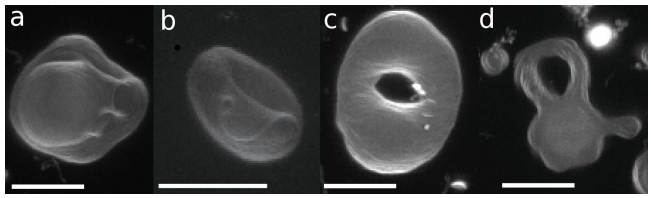

Fig. 2 Microscopy images of genus-1 liposomes. (a) Double-necked stomatycote. (b) Open stomatocyte. (c) Ellipsoidal toroid. (d) Discocyte with a tubular handle and arm. Scale bar: 10 μm.

Soft Matter Accepted Manuscript

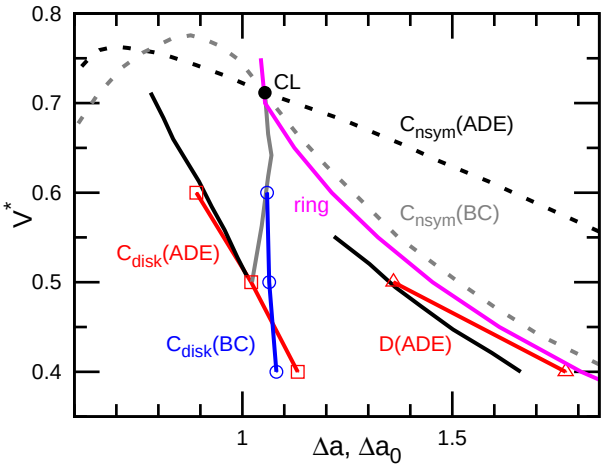

Fig. 3 Shape transition lines of the genus-1 vesicles with the ADE and BC models. The red and blue solid lines represent the shape transitions in ADE and BC models, respectively. C_{disk} and D represent the continuous and discrete transitions between open stomatocyte and disk and between elongated disk and circular toroid, respectively. The black and gray lines are ADE and BC boundaries extracted from Jülicher's phase diagrams in Ref.[13], respectively. The dashed lines represent phase boundaries between axisymmetric and non axisymmetric shapes (C_{nsym}). The filled circle represents the Clifford torus (CL). The magenta line represents the free-energy minimum states of the ring [the same as in Fig. 1(b)].

predicts these three types of the vesicles by minimizing the energy of the axisymmetric shapes. The circular toroid can be approximated by the revolution of a circle as follows:

$$\mathbf{r}(\theta,\phi) = ((r_1 + r_2\cos\phi)\cos\theta, (r_1 + r_2\cos\phi)\sin\theta, r_2\sin\phi). \quad (4)$$

In particular, the toroid with $r_1/r_2 = \sqrt{2}$ is the Clifford torus and has the lowest curvature energy $U_{Cl}/\kappa = 4\pi^2$ and $V^*_{CL} = 3/2^{5/4}\sqrt{\pi} \simeq 0.71$[10]. Note that thermal fluctuations give an additional curvature energy as $U_{cv} \simeq U_{CL} + (N_{mb} - 1)k_BT/2$ in the simulations because each bending mode is excited with $k_BT/2$. It was predicted that the ring vesicles are non-axisymmetric at $V^* > V^*_{CL}$ but axisymmetric at $V^* \leq V^*_{CL}$[11]. Our simulation results confirm their prediction for the ring. Although the circular shapes at $V^* \leq V^*_{CL}$ are not exactly axisymmetric, its deviation is small and can be understood as thermal fluctuations around the circular toroids. The area difference Δa of the revolution expressed in Eq. (4) is shown in the right black dashed line in Fig. 1(b). Our simulation results agree well with this estimation.

The axisymmetric double-necked stomatocyte (called a sickle-shaped toroid) is predicted as the global-minimum state at low V^* in the previous study[11]. In our simulations, two necks (or pores in the top view) of the stomatocyte are not typically along the center axis [see the left snapshot in Fig. 1(a)]. Experimentally observed double-necked stomatocytes are also off-center [see Fig. 2(a)]. The narrow neck shape is nearly catenoid, and its mean curvature is negligibly small. The energy difference between the axisymmetric and non-axisymmetric stomatocytes is small unless two necks are close to each other. The entropy of this diffusion is estimated as $S_{pore} \simeq k_B \ln(A/2d^2_{pore})$, where d_{pore} is the diameter of the pores and $A/2$ is the average area of inner and outer spherical components of stomatocyte. We obtain $S_{pore} \simeq 5k_B$ from $A = 820\sigma^2$ and $d_{sto} \simeq 2\sigma$ in our simulation. This is not a large value but it seems to be sufficient to overcome the energy difference. Thus, two necks can diffuse on the surface of the vesicle by thermal fluctuations. Vesicle deformation coupled with neck diffusion is observed. The membrane between two necks typically has large curvature [see Figs. 1(a) and 2(a)]. The entropy of these shape fluctuations and pore shape fluctuations[30] may also increase stability of non-axisymmetric shapes of the stomatocyte. The left black dashed line in Fig. 1(b) shows the values of Δa of stomatocytes modeled using two spheres. The shape deformation caused by thermal fluctuations slightly shift Δa to larger values.

The pore in the discocyte is also off-center. We discuss this in detail in the next subsection. In Jülicher's phase diagrams[13], the equilibrium shapes are axisymmetric in large region including the stomatocyte and ring (see Fig. 3). We will show non-axisymmetric equilibrium shapes in this region for low V^*.

Soft Matter Accepted Manuscript

This journal is © The Royal Society of Chemistry [year]

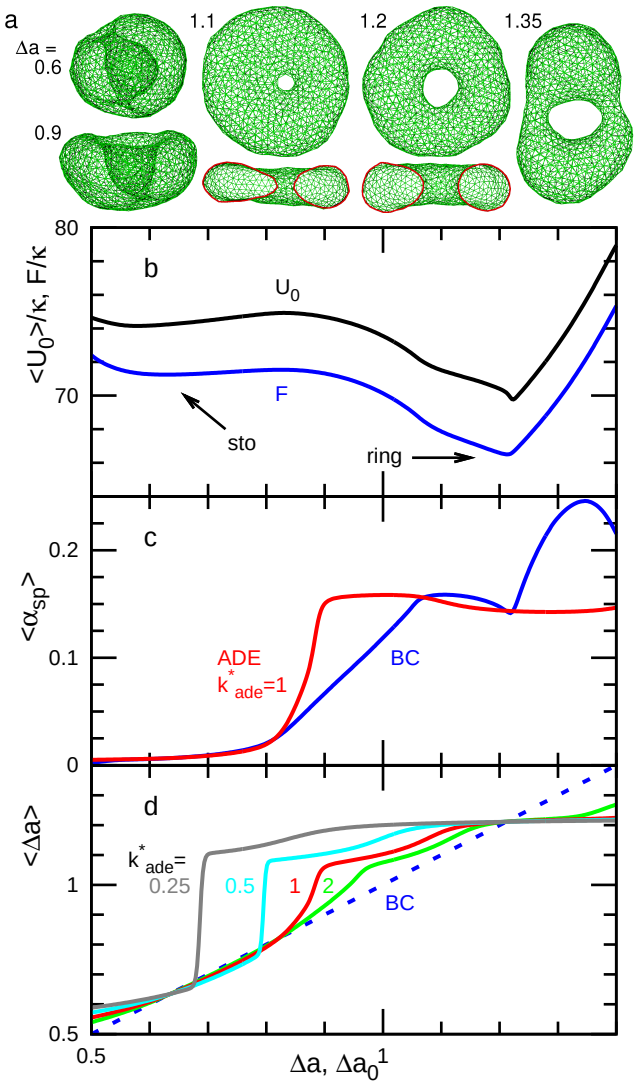

Fig. 4 Dependence of shape on Δa (BC) or Δa_0 (ADE) for genus-1 vesicles at $V^* = 0.6$. (a) Snapshots at $\Delta a = 0.6$, 0.9, 1.1, 1.2, and 1.35. The side views of half-cut snapshots are also shown at $\Delta a = 1.1$ and 1.2. (b) Free-energy profile F and mean potential energy $\langle U_0 \rangle$ for the BC model. (c) Mean asphericity $\langle \alpha_{sp} \rangle$ for the BC and ADE models with $k^*_{ade} = 1$. (d) Mean area difference $\langle \Delta a \rangle$. The solid lines represent the ADE models with $k^*_{ade} = 0.25$, 0.5, 1, and 2. The dashed line represents the BC model ($\langle \Delta a \rangle = \Delta a$). The error bars are smaller than the line thickness.

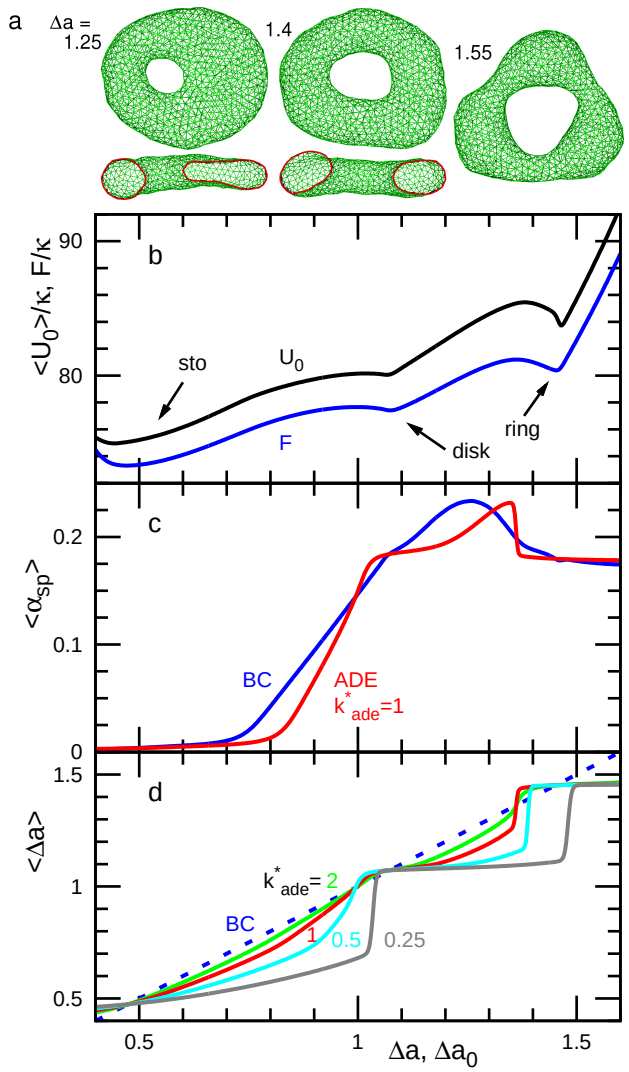

Fig. 5 Dependence of shape on Δa (BC) or Δa_0 (ADE) for genus-1 vesicles at $V^* = 0.5$. (a) Snapshots at $\Delta a = 1.25$, 1.4, and 1.55. The side views of half-cut snapshots are also shown at $\Delta a = 1.25$ and 1.4. (b) Free-energy profile F and mean potential energy $\langle U_0 \rangle$ for the BC model. (c) Mean asphericity $\langle \alpha_{sp} \rangle$ for the BC and ADE models with $k^*_{ade} = 1$. (d) Mean area difference $\langle \Delta a \rangle$. The data are presented in the same form as in Fig. 4.

Soft Matter Accepted Manuscript

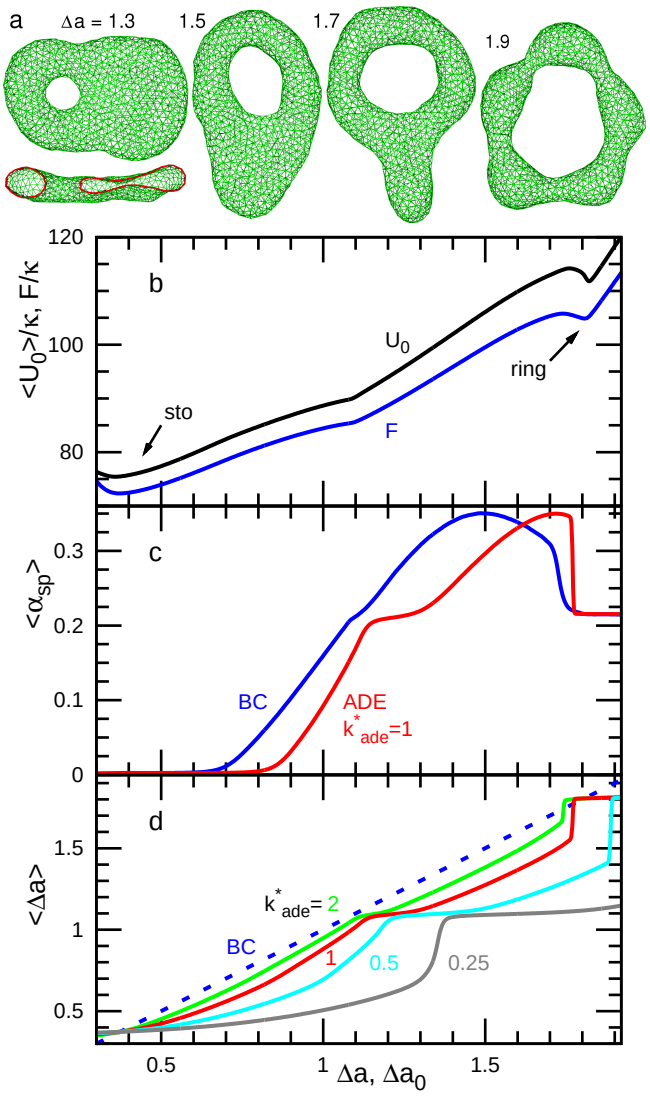

Fig. 6 Dependence of shape on Δa (BC) or Δa_0 (ADE) for genus-1 vesicles at $V^* = 0.4$. (a) Snapshots at $\Delta a = 1.3$, 1.5, 1.7, and 1.9. The side view of the half-cut snapshot at $\Delta a = 1.3$ is also shown. (b) Free-energy profile F and mean potential energy $\langle U_0 \rangle$ for the BC model. (c) Mean asphericity $\langle \alpha_{sp} \rangle$ for the BC and ADE models with $k^*_{ade} = 1$. (d) Mean area difference $\langle \Delta a \rangle$. The data are presented in the same form as in Fig. 4.

3.1.2 BC and ADE Models. To clarify the phase behavior of the genus-1 toroidal vesicle, the generalized ensemble MC simulations are performed at $V^* = 0.4$, 0.5, and 0.6 (see Figs. 3–6). The free-energy profiles F are calculated using probability distributions $P_{cv}(\Delta a)$ of the curvature energy model: $F(\Delta a) = -k_B T \ln(P_{cv}(\Delta a)) + C$. The constant C is unknown. Thus, we cannot obtain the absolute values of F but can compare its relative values. In Figs. 4–6(b), we shift F to be close to $\langle U_0 \rangle$ in order to make the comparison of two curves easier. The difference between Δa dependences of F and $\langle U_0 \rangle$ is caused by the entropy of membrane fluctuations.

To quantify the vesicle shapes, a shape parameter called asphericity, α_{sp}, is calculated. It is defined as[31]

$$\alpha_{sp} = \frac{(\lambda_1 - \lambda_2)^2 + (\lambda_2 - \lambda_3)^2 + (\lambda_3 - \lambda_1)^2}{2(\lambda_1 + \lambda_2 + \lambda_3)^2}, \qquad (5)$$

where $\lambda_1 \le \lambda_2 \le \lambda_3$ are the eigenvalues of the gyration tensor of the vesicle. The asphericity is the degree of deviation from a spherical shape; $\alpha_{sp} = 0$ for spheres, $\alpha_{sp} = 1$ for thin rods, and $\alpha_{sp} = 0.25$ for thin disks. The stomatocytes have $\alpha_{sp} \simeq 0$. The disk and ring shapes have $\alpha_{sp} \simeq 0.15$, 0.19, and 0.21 at $V^* = 0.6$, 0.5, and 0.4, respectively.

For $V^* = 0.6$ with increasing Δa, a neck of the stomatocyte opens, and subsequently the stomatocyte transforms into a discocyte (see Fig. 4). As Δa increases further, the pore in the discocyte becomes larger, and ultimately a circular toroid is formed. As Δa increases even further, the toroid elongates in one direction. This elongated shape is also observed in our experiment [compare Figs. 2(c) and 4(a)]. These transformations are continuous in both BC and ADE models with $k^*_{ade} \ge 1$. When the vesicle transforms from the discocyte to the open stomatocyte, mirror symmetry breaks, and the slops of $F(\Delta a)$ and the other quantities are changed. This is a second-order type of the transition, but the transition point is rounded by the finite energy increase. Since the curvature energy is independent of the vesicle size, the transition is not sharp even at $N_{mb} = \infty$. The area differences Δa and Δa_0 at this transition point are estimated from the second derivative of α_{sp} curves in Fig. 4(c). They agree with Jülicher's results for both ADE and BC models (see the curves denoted by C_{disk} in Fig. 3). The pore of the discocyte appears near the center of the disk. As the vesicle is annealed to $T = 0$, the pore moves to the center. Thus, it is considered that the stable shape is the axisymmetric discocyte predicted in Ref.[13] and that the discocyte is slightly deformed by thermal fluctuations. The discocyte does not have a minimum in the free-energy profile in Fig. 4(b), and no clear transitions are observed between the discocyte and circular toroid. The neck in the open stomatocyte can also be off-center. Such a non-axisymmetric open stomatocyte is experimentally observed, as shown in Fig. 2(b).

At $V^* = 0.5$, the vesicle transforms from a stomatocyte to a circular toroid via a discocyte [see Figs. 1(a) and 5]. The

Soft Matter Accepted Manuscript

This journal is © The Royal Society of Chemistry [year]

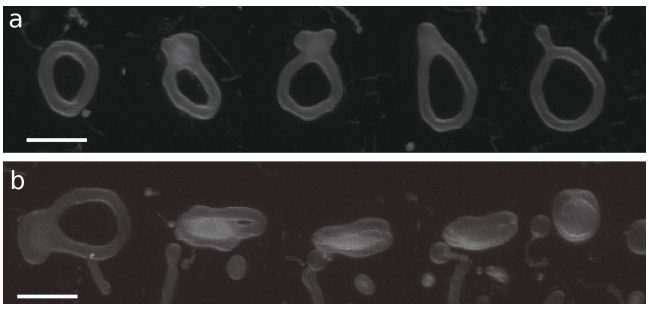

Fig. 7 Time-sequential microscopy images of genus-1 liposomes. (a) Transformation from a circular toroid to racket shape via a handled discocyte. From left to right: $t = 0$, 160, 180, 188, and 192 s. (b) Transformation from a handled discocyte to stomatocyte via a discocyte with a small pore and open stomatocyte. From left to right: $t = 0$, 62, 80, 91, and 131 s. Scale bar: 10 μm.

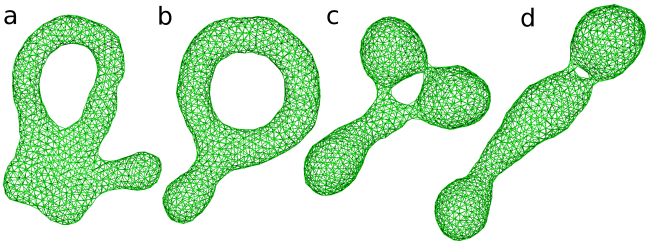

Fig. 8 Snapshots of genus-1 vesicles. (a) $(V^*, \Delta a_0) = (0.3, 2.2)$. (b) $(V^*, \Delta a_0) = (0.4, 1.9)$. (c) $(V^*, \Delta a_0) = (0.5, 2.2)$. (d) $(V^*, \Delta a_0) = (0.5, 2.2)$.

difference from $V^* = 0.6$ is that the discocyte is at a minimum of $F(\Delta a)$ and non-axisymmetric elongated discocytes appear between two energy minima of the discocyte and ring. In the stable discocyte [the middle snapshot in Fig. 1(a)], the pore is off-center and stays on the edge of the dimple. As the vesicle is annealed to $T = 0$, the pore remain on the edge. We also confirmed the formation of these non-axisymmetric discocytes at $N_{\rm mb} = 4000$. Michalet and Bensimon experimentally observed this off-center discocyte[18]. They reported that it is an energy minimum state by using the energy minimization, but they did not clarify whether it is the global- or local- minimum state[18]. Our simulation revealed that the off-center discocyte is the global-minimum state in both BC and ADE models. In the axisymmmetric discocyte, the pore opens in the almost flat membranes at the middle of the dimples. As the pore approaches the edge of the dimples, the curvature of the edge is partially reduced. Similar pore formations on the edge of the highly curved structures are obtained in membrane-fusion intermediates. The fusion pore opens at the edge of hemifusion diaphragm[32,33] and at the side of a stalk neck connecting two bilayer membranes[34,35].

As Δa increases at $V^* = 0.5$, the pore in the disocyte is expanded at this off-center position, and the vesicle becomes an elliptic discocyte [see the left snapshot in Fig. 5(a) and the peak at $\Delta a = 1.25$ in Fig. 5(c)]. In the BC model, the vesicle then becomes a circular toroid via an elongated circular toroid [see the middle snapshot in Fig. 5(a)]. In contrast, in the ADE model with $k^*_{\rm ade} = 1$, the vesicle exhibits a discrete transition from an elliptic discocyte to a circular toroid at $\Delta a_0 = 1.36$. This transition point agrees with the prediction in Ref.[13] (see Fig. 3), despite the fact that only axisymmetric shapes are considered in Ref.[13]. This good agreement might be due to the small energy difference between the axisymmetric discocyte and elliptic discocyte.

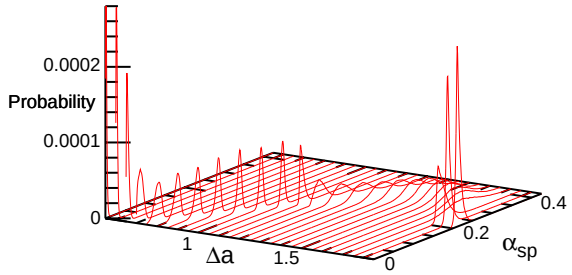

Fig. 9 Probability distribution of asphericity $\alpha_{\rm sp}$ for genus-1 vesicles in the BC model at $V^* = 0.4$.

At $V^* = 0.4$, the vesicle forms pronounced non-axisymmetric shapes between the off-center circular discocyte and circular toroid (see Fig. 6). The pore is not in the dimples of the discocyte but outside of the discotye, which is similar to a handle, as shown in the right snapshot in Fig. 6(a). We also observed this shape experimentally (see the left images in Fig. 7). Such handled discocyte has not been reported previously. With decreasing V^*, the elliptic discocyte becomes more elongated, and subsequently the large flat parts form dimples. As Δa increases, the pore becomes larger and the discoidal part becomes narrower. When Δa is further increased in the BC model, the vesicles form a tubular arm similar to the grip of a racket [see Fig. 6(a)] and subsequently becomes a circular toroid. In the ADE model, the racket-shaped vesicle is skipped in the phase diagram, and a discrete transition from the elongated handled discocyte of $\Delta a = 1.25$ to the circular toroid of $\Delta a = 1.81$ occurs at $\Delta a_0 = 1.77$ [see Fig. 6(c)]. The transition point is slightly shifted from the previous prediction for the transition from axisymmetric disk and ring[13] (see Fig. 3), because of a large deviation of the discocyte from the axisymmetric shape. The racket-shaped vesicle exists as a local-minimum state at larger values of Δa_0 [see Fig. 8(b)]. In the experiment, a handled discocyte with a tubular arm is observed [see Fig. 2(d)]. A similar shape is obtained as a local energy-minimum state in the ADE model [see Fig. 8(a)]. A circular toroid connecting two tubular arms is also obtained (data not shown). At low V^*, tubular arms often remain once

Soft Matter Accepted Manuscript

they are formed such that several local-minimum states appear.

Figure 7 shows time-sequential microscopy images of shape transformations of genus-1 vesicles. These transformations from a handled discocyte to a racket shape and stomatocyte are well explained by gradual changes of Δa_0 at $V^* = 0.3$: from $\Delta a_0 = 2.2$ to 2.6 [Fig. 7(a)] and from $\Delta a_0 = 2.3$ to 0.6 [Fig. 7(b)], respectively. Movies of corresponding simulations are provided in ESI (Movies 1 and 2).

The entropy of the shape fluctuations slightly modifies the phase behavior. The area difference Δa at the minimum free energy is smaller than that at the minimum of the mean potential energy $\langle U_0 \rangle$ by 0.01 at $V^* = 0.5$. The entropy of the shape fluctuations is large for the elongated discocyte because the difference of the curves $\langle U_0 \rangle$ and F are large at $\Delta a \simeq 1.4$ and 1.75 at $V^* = 0.5$ and 0.4, respectively. The fluctuations of asphericity $\alpha_{\rm sp}$ are also large in these regions, and $\alpha_{\rm sp}$ exhibits broad distributions, as shown in Fig. 9.

We have shown the discrete transition between elongated discocyte and circular toroid at $V^* = 0.5$ and 0.4 for the ADE model with $k^*_{\rm ade} = 1$. The transformation between stomatocyte and discocyte becomes a discrete transition at lower values of $k^*_{\rm ade}$ [see Figs. 4(d) and 5(d)]. With decreasing V^*, a lower value of $k^*_{\rm ade}$ is needed to obtain the discrete transition. Thus, the values of $k^*_{\rm ade}$ may be estimated by systematically observing the transformation dynamics under changes in Δa_0 or V^*.

As Δa increases further from the circular toroid, the toroid deforms into ellipsoid, triangle, and pentagon at $V^* = 0.6$, 0.5, and 0.4, respectively. Thus, a higher undulation mode becomes unstable and grows at lower values of V^*. When the vesicle is approximated as the circular revolution expressed in Eq. (4), the length ratio of two circumferences are $r_1/r_2 =$ 1.99, 2.86, and 4.48 at $V^* = 0.6$, 0.5, and 0.4, respectively. Therefore, the unstabilized mode is determined by the wavelength of $2\pi r_2$. When $r_1/r_2 \to \infty$, the toroid is approximated as a cylinder of radius r_2. It is known that for cylindrical membranes of spontaneous curvature C_0 the undulation mode of wavelength $2\pi r_2$ becomes unstable at $C_0 r_2 = 1$ [36]. Our simulation results show that this relation holds for finite values of r_1/r_2.

3.1.3 Budding. The toroidal vesicles exhibit a budding transition in a manner similar to genus-0 vesicles. The area difference Δa at the budding transition for $g = 1$ is shown as a green line in Fig. 1(b). This line is obtained though canonical MC simulations of the ADE model. The budding is a discrete transition, and the error bars show the hysteresis regions, where budded or unbudded shapes are obtained on the basis of initial vesicle conformations. The intrinsic area difference Δa_0 at the transition points are larger than Δa: $\Delta a_0 = 2.6 \pm 0.1$ and 1.29 ± 0.02 at $V^* = 0.3$ and 0.75, respectively. An example of the budding transition is shown in Fig. 10. Our simulation

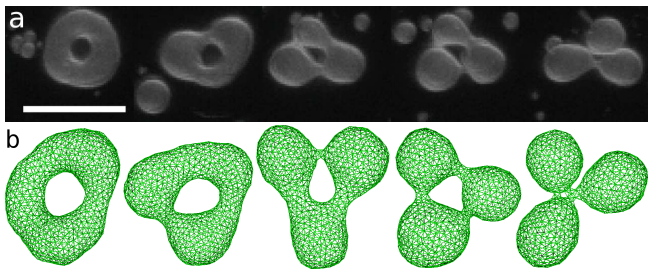

Fig. 10 Shape transformations of a genus-1 vesicle at $V^* = 0.55$. (a) Time-sequential microscopy images of liposomes. From left to right: $t = 0$, 45, 95, 97, and 144 s. Scale bar: 10 μm. (b) Sequential snapshots of the triangulated-membrane simulation. Intrinsic area difference Δa_0 is gradually increased with $d\Delta a_0/dt = 1 \times 10^{-8}$, where t represents MC steps. From left to right: $\Delta a_0 = 1.73$, 1.8, 1.87, 1.97, and 2.35.

reproduces the dynamics of the liposome very well.

Since the budded compartments are divided by small necks, large free-energy barriers can exist between meta-stable and stable states. Thus, it is difficult to identify the most stable state. The snapshots in Figs. 8(c) and (d) show two free-energy-minimum states at $(V^*, \Delta a_0) = (0.5, 2.2)$. The triangular and straight shapes are typically obtained as Δa_0 increases and as V^* decreases, respectively. These two shapes have almost identical potential energy with $\langle U \rangle / \kappa = 120$. As Δa_0 gradually decreases from $\Delta a_0 = 2.2$, the straight shape is retained better than the triangular budded shape at lower values of Δa_0. A bud connected by two necks appears to be more robust than one connected by a single neck. To calculate the free energies using a generalized ensemble method, order parameters to connect these budded states and circular toroid are required. However, typical shape parameters such as $\alpha_{\rm sp}$ are not suitable, since the budding occurs in local regions of the vesicle.

3.2 Genus-2 Toroidal Vesicles

The genus-2 vesicles form closed and open stomatocytes, discocytes, and budded shapes (see Figs. 11 and 12). These shapes are similar to those of genus-1 vesicles described in the previous section. A significant difference is that no axisymmetric shapes exist for $g = 2$. Two pores cannot align at the center of the discocyte.

A discocyte with two handles is observed experimentally. The time-sequential shape transformation from a budded toroid to handled discocyte is well reproduced by our simulation [compare Figs. 12(a) and (b)].

The size of two pores in the vesicles can be different. An extreme example is shown in Figs. 11(a,iii) and (b,v). The ends of a tubular vesicle are connected by two necks. This shape is metastable and obtained in the region slightly below

Soft Matter Accepted Manuscript

This journal is © The Royal Society of Chemistry [year]

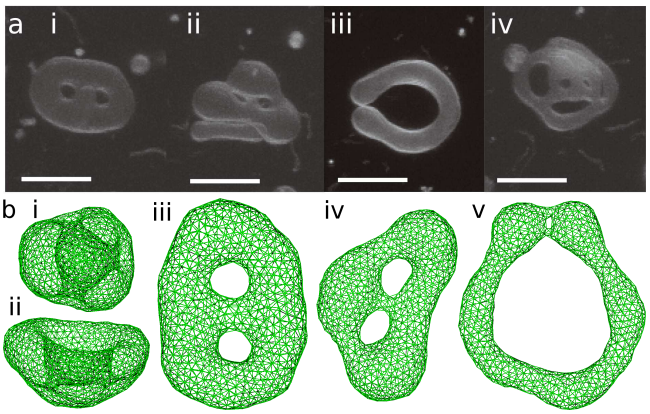

Fig. 11 (a) Microscopy images of liposomes of (i–iii) $g = 2$ and (iv) $g = 5$. Scale bar: 10 μm. (b) Snapshots for the toroidal vesicle of $g = 2$. (i) $(V^*, \Delta a_0) = (0.5, 0.8)$. (ii) $(V^*, \Delta a_0) = (0.5, 1)$. (iii) $(V^*, \Delta a_0) = (0.5, 1.5)$. (iv) $(V^*, \Delta a_0) = (0.5, 1.8)$. (v) $(V^*, \Delta a_0) = (0.35, 2.7)$.

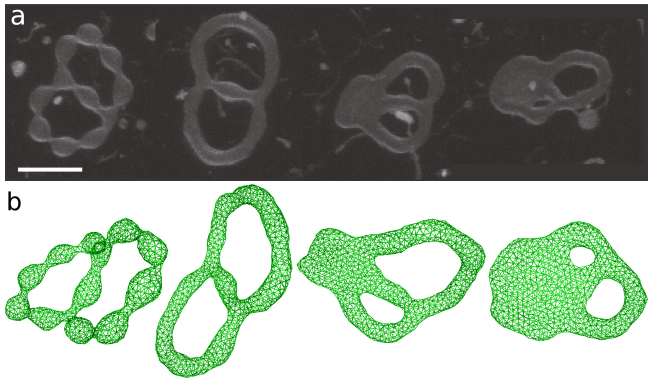

Fig. 12 Shape transformations of a genus-2 vesicle at $V^* = 0.25$. (a) Time-sequential microscopy images of liposomes. From left to right: $t = 0$, 84, 197, and 244 s. Scale bar: 10 μm. (b) Sequential snapshots of the triangulated-membrane simulation. Intrinsic area difference Δa_0 is gradually decreased with $d\Delta a_0/dt = 2 \times 10^{-8}$. From left to right: $\Delta a_0 = 4$, 3.46, 2.6, and 2.

the budding transition. At $g > 2$, more complicated shapes are expected. Figure 11(a,iv) shows an example of genus-5 liposomes.

4 Conclusions

Various morphologies of the genus-1 and 2 toroidal vesicles are clarified numerically and experimentally. For $g = 1$, new stable non-axisymmetric shapes are revealed from the free-energy profile calculation. As Δa increases at $V^* = 0.5$, a circular discocyte with an off-center pore transforms into an elliptic discocyte and then into a circular toroid. At $V^* = 0.4$, between the circular discocyte and circular toroid, the discocyte with a handle and racket shape are formed. The discrete transition occurs between the elliptic discocyte and circular toroid in the ADE model. The handled discocytes are also observed for $g = 2$. As increasing Δa further, the formation of polygonal toroidal vesicles and subsequential budding are also found. Number of polygon edges are increased with decreasing V^* and are understood by the bending instability. Our simulation results agree with our experimental observation very well. The following shapes are experimentally observed for the fist time: Stomatocytes and racket-shaped vesicle for genus-1 and handled discocytes for genus-1 and 2.

As the genus of vesicles increases, the regions of non-axisymmetric shapes are expanded in the phase diagram. For $g = 1$, the non-axisymmetric discocytes are stable in the region where the axisymmetric discocytes are formed for $g = 0$. For $g = 2$, all of obtained shapes are non-axisymmetric. Although the phase diagram of the genus-2 vesicles is investigated on the basis of symmetry analyses in Refs.[14,15], thermal fluctuations are neglected. A hexagonal array of pores is observed in polymersomes[37]. Shape transformations of the vesicles of genus 2 and higher under thermal fluctuations are an interesting problem for further studies.

Acknowledgments

The authors would like to thank G. Gompper for informative discussions. This work was partially supported by a Grant-in-Aid for Scientific Research on Innovative Areas "Fluctuation & Structure" (No. 25103010) from the Ministry of Education, Culture, Sports, Science, and Technology of Japan. The numerical calculations were partly carried out on SGI Altix ICE 8400EX at ISSP Supercomputer Center, University of Tokyo.

References

1 *Structure and Dynamics of Membranes*, ed. R. Lipowsky and E. Sackmann, Elsevier Science, Amsterdam, 1995.
2 R. Lipowsky, *Stastical mechanics of biocomplexity*, Springer, Berlin, 1999, vol. 527, pp. 1–23.
3 U. Seifert, *Adv. Phys.*, 1997, **46**, 13–137.
4 S. Svetina and B. Žekš, *Anat. Rec.*, 2002, **268**, 215–225.
5 S. Svetina and B. Žekš, *Euro. Biophys. J.*, 1989, **17**, 101–111.
6 N. Khalifat, N. Puff, S. Bonneau, J.-B. Fournier and M. I. Angelova, *Biophys. J.*, 2008, **95**, 4924 – 4933.
7 H. Noguchi, *J. Phys. Soc. Jpn.*, 2009, **78**, 041007.
8 A. Sakashita, N. Urakami, P. Ziherl and M. Imai, *Soft Matter*, 2012, **8**, 8569–8581.
9 A. Sakashita, M. Imai and H. Noguchi, *Phys. Rev. E*, 2014, **89**, 040701(R).
10 Z. C. Ou-Yang, *Phys. Rev. A*, 1990, **41**, 4517–4520.
11 U. Seifert, *Phys. Rev. Lett.*, 1991, **66**, 2404–2407.
12 B. Fourcade, M. Mutz and D. Bensimon, *Phys. Rev. Lett.*, 1992, **68**, 2551–2554.

Soft Matter Accepted Manuscript

13 F. Jülicher, U. Seifert and R. Lipowsky, *J. Phys. II (France)*, 1993, **3**, 1681–1705.
14 F. Jülicher, U. Seifert and R. Lipowsky, *Phys. Rev. Lett.*, 1993, **71**, 452–455.
15 F. Jülicher, *J. Phys. II (France)*, 1996, **6**, 1797–1824.
16 X. Michalet, D. Bensimon and B. Fourcade, *Phys. Rev. Lett.*, 1994, **72**, 168–171.
17 X. Michalet and D. Bensimon, *Science*, 1995, **269**, 666–668.
18 X. Michalet and D. Bensimon, *J. Phys. II (France)*, 1995, **5**, 263–287.
19 X. Michalet, *Phys. Rev. E*, 2007, **76**, 02914.
20 A. Yamamoto and M. Ichikawa, *Phys. Rev. E*, 2012, **86**, 061905.
21 G. Gompper and D. M. Kroll, *J. Phys. Condens. Matter*, 1997, **9**, 8795–8834.
22 G. Gompper and D. M. Kroll, *Statistical Mechanics of Membranes and Surfaces*, World Scientific, Singapore, 2nd edn, 2004.
23 P. B. Canham, *J. Theor. Biol.*, 1970, **26**, 61–81.
24 W. Helfrich, *Z. Naturforsch*, 1973, **28c**, 693–703.
25 C. Itzykson, Proceedings of the GIFT seminar, Jaca 85, Singapore, 1986.
26 H. Noguchi and G. Gompper, *Phys. Rev. E*, 2005, **72**, 011901.
27 Y. Okamoto, *J. Mol. Graph. Model.*, 2004, **22**, 425–439.
28 B. A. Berg, H. Noguchi and Y. Okamoto, *Phys. Rev. E*, 2003, **68**, 036126.
29 A. M. Ferrenberg and R. H. Swendsen, *Phys. Rev. Lett.*, 1988, **61**, 2635–2638.
30 O. Farago and C. D. Santangelo, *J. Chem. Phys.*, 2005, **122**, 044901.
31 J. Rudnick and G. Gaspari, *J. Phys. A: Math. Gen.*, 1986, **19**, L191–L193.
32 H. Noguchi, *J. Chem. Phys.*, 2002, **117**, 8130–8137.
33 H. Noguchi, *Soft Matter*, 2012, **8**, 3146–3153.
34 H. Noguchi and M. Takasu, *J. Chem. Phys.*, 2001, **115**, 9547–9551.
35 M. Müller and M. Schick, *Curr. Top. Membr.*, 2011, **68**, 295–323.
36 Z. C. Ou-Yang and W. Helfrich, *Phys. Rev. A*, 1989, **39**, 5280–5288.
37 C. K. Haluska, W. T. Góźdź, H.-G. Döbereiner, S. Förster and G. Gompper, *Phys. Rev. Lett.*, 2002, **89**, 238302.

Soft Matter Accepted Manuscript

This journal is © The Royal Society of Chemistry [year]